

Shaping and Locomotion of Soft Robots Using Filament Actuators Made from Liquid Crystal Elastomer–Carbon Nanotube Composites

Jiaqi Liu, Yuchong Gao, Haihuan Wang, Ryan Poling-Skutvik, Chinedum O. Osuji, and Shu Yang*

Soft robots, with their agile locomotion and responsiveness to environment, have attracted great interest in recent years. Liquid crystal elastomers (LCEs), known for their reversible and anisotropic deformation, are promising candidates as embedded intelligent actuators in soft robots. So far, most studies on LCEs have focused on achieving complex deformation in thin films over centimeter-scale areas with relatively small specific energy densities. Herein, using an extrusion process, meter-long LCE composite filaments that are responsive to both infrared light and electrical fields are fabricated. In the composite filaments, a small quantity of cellulose nanocrystals (CNCs) is incorporated to facilitate the alignment of liquid crystal molecules along the long axis of the filament. Up to 2 wt% carbon nanotubes (CNTs) is introduced into a LCE matrix without aggregation, which in turn greatly improves the mechanical property of filaments and their actuation speed, where the Young's modulus along the long axis reaches 40 MPa, the electrothermal response time is within 10 s. The maximum work capacity is 38 J kg^{-1} with 2 wt% CNT loading. Finally, shape transformation and locomotion in several soft robotics systems achieved by the dual-responsive LCE/CNT composite filament actuators are demonstrated.

changes, limiting their capabilities to work intelligently and complete complex tasks as bio-organisms do.^[1] Soft robots that are light-weight, offering additional degrees of freedom and compliance are attractive. However, their softness could also make it difficult to control the shape change and locomotion, or lift heavy weights. To precisely and locally control the shapes and locomotion with considerable strain requires embedded intelligence. Recently, functional soft materials such as environmentally responsive hydrogels,^[2] shape memory polymers (SMPs),^[3] and liquid crystal elastomers (LCEs)^[4] have been extensively studied. Compared with the isotropic deformation of hydrogels and conventional SMPs, the intrinsic anisotropy of liquid crystals (LCs) coupled with rubber elasticity in LCEs make them superior as actuators for more forceful and faster responses yet at lower energy cost. Above the nematic to isotropic phase transition


1. Introduction

Conventional robots are made of rigid materials such as metal. Although they can be designed to complete sophisticated tasks by incorporating multiple motors or pneumatical systems, they are often heavy, tethered, and nonadaptive to environmental

temperature (T_{NI}), due to the anisotropic mechanical property of the LCE networks, the network contract along the LC director field and expand in the perpendicular direction (Figure 1a),^[4] leading to reversible and anisotropic shape deformation with up to 500% strain.^[5] The actuation of LCEs depends on the molecular alignment of LCs in the network. Nearly all compressive strain leads to extension in the perpendicular direction (or soft direction) of LCEs. As elastic energy density of deformation is quadratic in strain, the energy input requirement in the soft direction will be minimal. Meanwhile, if we can control the intrinsic anisotropy, we can pre-program the actuation. We note that the spatial control of LC director fields is essential to realize complicated deformation within a monolithic LCE. Several methods have been developed to realize spatial control of LC alignment in thin films ($\approx 100 \mu\text{m}$ thick and a few centimeter wide/long) to achieve complex actuation modes, including microchannels,^[6–8] photoalignment,^[9–11] and 3D printing.^[12–15] However, the thin-film based actuators are highly confined by the substrates they are prepared from, which, here, determine the orientation of LC molecules and the overall sample dimension, thus, limiting the scalability and integration of the actuators with the soft robots at an arbitrary location.

J. Liu, Y. Gao, H. Wang, Prof. S. Yang
Department of Materials Science and Engineering
University of Pennsylvania
3231 Walnut Street, Philadelphia, PA 19104, USA
E-mail: shuyang@seas.upenn.edu

Dr. R. Poling-Skutvik, Prof. C. O. Osuji
Department of Chemical and Biomolecular Engineering
University of Pennsylvania
220 South 33rd Street, Philadelphia, PA 19104, USA

 The ORCID identification number(s) for the author(s) of this article can be found under <https://doi.org/10.1002/aisy.201900163>.

© 2020 The Authors. Published by WILEY-VCH Verlag GmbH & Co. KGaA, Weinheim. This is an open access article under the terms of the Creative Commons Attribution License, which permits use, distribution and reproduction in any medium, provided the original work is properly cited.

DOI: 10.1002/aisy.201900163

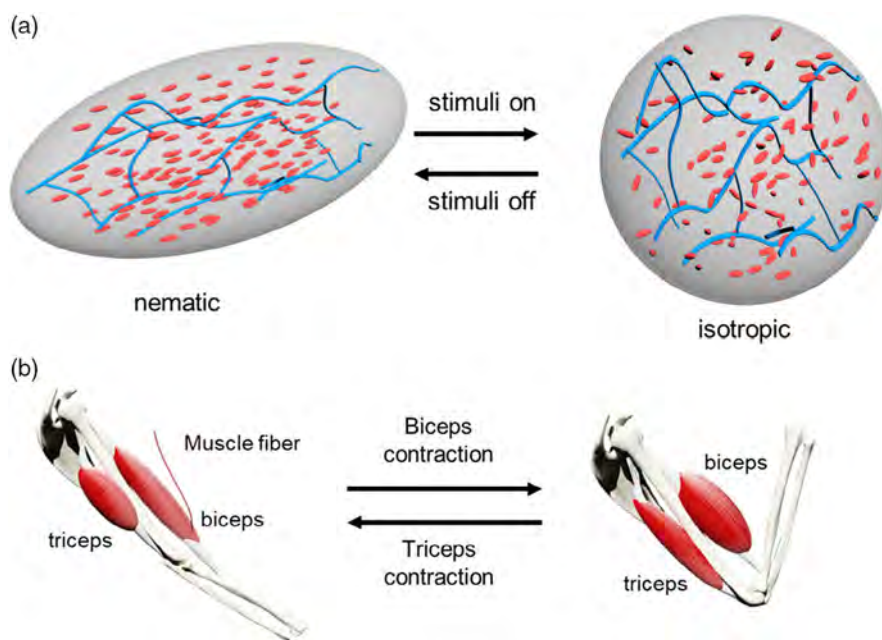


Figure 1. Design concept for LCE/CNT composite filaments as soft robots. a) LCE working mechanism as actuator. b) Muscle-like soft actuator.

Work capacity is another important parameter to be considered for advanced soft robots. It describes the amount of work an actuator can generate within a fixed period of time. The earlier versions of soft robots cannot sustain heavy objects such as the conventional rigid robots. Due to the intrinsic compliance of soft materials (modulus in the range of 10^4 – 10^9 Pa),^[1] they often lack the desired mechanical strength to generate high work capacity and LCEs are no exceptions. Several efforts have been made to increase the work capacity of LCE actuators, including forming interpenetrating double networks of LCE and LC thermoset,^[16] laying up carbon nanotube (CNT) sheets on LCE films,^[17] and stacking multiple layers of LCE films.^[11] Nevertheless, multi-step fabrication processes are required. More importantly, the sample size has been restricted to centimeter scales. A scalable, facile method to fabricate LCE actuators with both controllable deformation and large work capacity is highly desired.

Notably, the agile yet forceful locomotion by human and animals are usually enabled by the musculoskeletal system, where rigid bones provide support and stability, contractible muscles offer stretching ability, and the connecting tissues such as tendons and ligaments offer flexibility (Figure 1b). The work capacity of human muscle can reach 40 J kg^{-1} with a maximum strain over 40%.^[18] To mimic both the dexterity and robustness in the musculoskeletal system, we extrude meter-long LCE filament-based actuators. To increase the mechanical strength of the filaments, we add cellulose nanocrystals (CNCs) and CNTs. Based on the photothermal effect of CNTs and the Joule heating effect of copper wires, we show that the LCE/CNT composite filaments exhibit both infrared (IR)-light and electrothermal responsiveness, while achieving large work capacity (38 J kg^{-1} with 2 wt% CNT loading) and fast response time. We show that the filaments can be laid into arbitrary patterns for shape transformation or integrated in different robotic systems,

demonstrating a photoresponsive hopping unicorn, an electrothermally responsive flying eagle, and a multifunctional swing set with three locomotion modes.

2. Results and Discussion

2.1. Scalable Fabrication of LCE/CNT Composite Filaments

We formulate an LCE/CNT ink (Figure 2a) that can be extruded at room temperature while maintaining LC alignment along the extrusion path with a large nozzle diameter (inner diameter ID = $900 \mu\text{m}$). To enable the extrusion process at room temperature, we choose the LC chemistry based on an oxygen-mediated thiol-acrylate click reaction reported earlier.^[7] First, we pre-oligomerize the diacrylate (1,4-bis-[4-(6-acryloyloxyhexyloxy)benzoyloxy]-2-methylbenzene, known as RM82) with a short chain dithiol 1,3-propane dithiol (1,3 PDT) through a base-catalyzed click reaction to obtain a mixture of thiol-terminated oligomers, referred as RM82–1,3 PDT. The 1:1 molar ratio mixture of LC oligomers RM82–1,3 PDT and RM82 show a large nematic window covering the room temperature, and can be UV crosslinked via the free-radical polymerization to lock the LC molecular alignment along the extruded direction within several seconds. The LCE ink is first heated at $80 \text{ }^\circ\text{C}$ for 30 min before extrusion to obtain the favorable viscoelastic behavior^[12,19] and then cooled down to room temperature for extrusion.

Unlike 3D printing of LCEs, where the nozzle ID has to be $150 \mu\text{m}$ or smaller,^[13,14] here we are able to extrude filaments with a diameter of $860 \mu\text{m}$ without deteriorating LC molecular alignment. We compare filaments extruded from nozzles of different ID (Figure S1, Supporting Information), and show well-aligned filaments can be extruded from the nozzle of ID as large as $900 \mu\text{m}$, comparable with those obtained from $500 \mu\text{m}$ ID

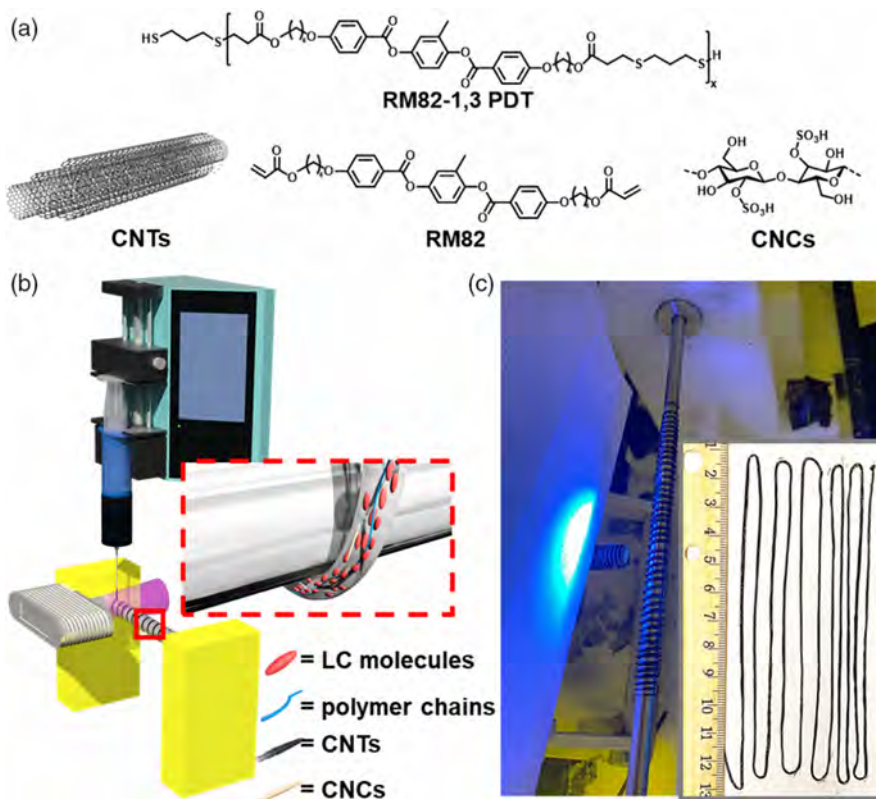


Figure 2. Fabrication of LCE/CNT composite filaments. a) Chemical structures of LC materials RM82 and RM82-1,3 PDT, and schematic illustrations of CNCs and CNTs. b) Schematic illustration of the fabrication process. c) Digital images of obtained LCE/CNT composite filaments. Inset: a 1.4-m-long filament.

nozzle (Figure S2, Supporting Information) due to small addition of CNCs and extremely efficient UV crosslinking. Our capability of fabricating actuable LCE filaments with large diameters is essential for large-scale soft robotic applications. When adding up to 2 wt% multiwalled CNTs (MWCNTs), we not only enhance the mechanical strength and work capacity of LCE filaments but also improve the actuation speed and provide IR-light responsiveness.

The extrusion process of the LCE/CNT composite filaments is shown in Figure 2b. The LCE ink is extruded at a constant rate of $50 \mu\text{L min}^{-1}$ by a syringe pump, where the pump is fixed in an upright position to eliminate the gravity effect and improve the uniformity of filaments. Once the ink is extruded out of the nozzle, it is exposed to UV light for a few seconds, same as the process for pure LCE filament, to lock the LC alignment and the filament shape, followed by collection from a rotating mandrel (2 rad min^{-1}) at the bottom. The shear force during extrusion induces the LC molecular order along the extrusion path (inset of Figure 2b), enabling the large deformation of LCE/CNT composite filaments along the filament's long axis. When extrusion is completed, the filaments are removed from the mandrel and fully crosslinked by an additional flood UV exposure at a total dosage of 100 J cm^{-2} . This fabrication method is facile and stable, hence readily scaled-up. As shown in Figure 2c, a 1.4-m-long LCE/CNT filament with rather uniform diameter is fabricated continuously in a single extrusion process without breakage.

Due to the large van der Waals interactions, CNTs tend to aggregate together, which will not only influence the viscosity and shear-thinning behavior of the mixture^[20] but also cause nonuniform distribution of CNTs and breakage of filament during extrusion. As shown in the cross-sectional scanning electron microscopy (SEM) images (Figure S3, Supporting Information), the CNTs distribute uniformly without aggregation inside the composite filament even at a 2 wt% concentration. Previously, it has been reported that CNTs aggregated as low as 0.1 wt% in LCE films.^[17,21,22] We believe that the much higher loading in our system could be attributed to the shearing force during extrusion. Supporting this is when we attempt to fabricate LCE/CNT composite films by capillary infiltration of the same LCE/CNT ink into a glass cell, aggregation of CNTs does occur. The much improved loading of CNTs in LCE matrix allows us to improve the mechanical robustness of filaments without sacrificing the actuation strain and realize better actuation performance for soft robotics.

2.2. The Role of Nanofillers in Muscle-Like LCE/CNT Composite Filaments

Our ability to fabricate LCE/CNT composite filaments with well-aligned LC molecules through extra-large nozzle ($900 \mu\text{m ID}$) is mainly attributed to the addition of nanofiller CNCs. It is known that CNCs are needle-shaped rigid molecules and can form

lyotropic LC phases at high concentrations.^[23,24] When functionalized with surface groups, herein sulfonate, the charge repulsion between each other will keep the CNCs separated, hence facilitating the alignment of LC molecules during the extrusion process. To explore the role of CNCs, we prepare three different samples with fixed CNT concentration (1 wt%) and vary the CNC concentrations, 0, 2 and 4 wt%. We characterize the alignment of composite filaments by wide-angle X-ray diffraction (WAXRD). In 2D WAXRD patterns, polydomain LCEs exhibit a uniform diffraction ring, whereas uniaxially aligned LCEs exhibit two high-intensity arc areas on the diffraction ring. As shown in Figure S4, Supporting Information, the diffraction pattern changes from a nearly isotropic ring to two distinct arcs with increasing CNC concentration. When we integrate the intensity from the 2D WAXRD patterns as a function of azimuthal angle ψ (Figure 3a), the maximum peak intensity clearly increases with CNC concentrations, indicating the formation of better aligned nematic phase in the filaments. The appearance of peaks around 90° and 270° suggests that the nematic directors are along 0° and 180° , which is the long axis of the filament. This trend, however, cannot be further explored as CNC concentration is greater than 4 wt%, where the viscosity of LCE ink increases dramatically, hindering the continuous fabrication of uniform composite filaments. As a result of better alignment with increasing CNC concentrations, the filament with 4 wt% CNC can withstand 15% more strain (from 35% to more than 50%) without diminishing the Young's modulus (around 24 MPa) according to the tensile test (Figure 3b). The filament with higher CNC loading becomes more stretchable, which will also lead to larger deformation strain and benefit the actuation performance. Therefore, we keep 4 wt% CNC doping concentration for all the following experiments.

We now turn our attention to the role of CNTs as nanofillers in the composite filament. We add CNTs up to 2 wt%; similar to the case of CNCs, when loading of CNTs exceeds 2 wt%, the ink also becomes drastically viscous, clogging the nozzle during extrusion. Higher CNT concentrations would also hinder the rapid crosslinking of filaments, as CNTs absorb strongly in the UV region. CNTs are known for ultra-high mechanical strength and thermal and electrical conductivity, and thus they have been commonly used in polymer composites.^[17,21,22] As shown in the

stress–strain curves in Figure 3c, increase in CNT concentrations leads to larger modulus (or steeper slope), higher maximum stress, and increased stiffness (or lower strain-at-break). At 2 wt% CNT loading, the LCE composite filament becomes somewhat brittle, which breaks at 41% strain, whereas the one with no CNTs can endure 53% strain. Meanwhile, the Young's modulus of the composite filaments increases nearly fourfold, from 11 to 40 MPa, when CNT concentration increases from 0 to 2 wt%. Combining the rigid CNTs with the soft elastomeric LCE matrix, the composite filaments are significantly reinforced to exhibit much larger modulus at the expense of a small amount of strain-at-break.

2.3. Work Capacity and Actuation Performance

In addition, CNTs contribute to the photothermal responsiveness of composite filaments.^[25] The ability of CNTs to absorb multiple wavelength light, especially in the IR region, and release in the form of heat,^[26] i.e., photothermal effect, can trigger the phase transition of LCE/CNT composite filaments under broad-band IR irradiation by raising the temperature above T_{NI} . As a result, LC molecules become isotropic and the composite filament shrinks along the long axis. When the IR light source is removed and heat dissipates, the LCE network returns to the nematic phase and the filament recovers to the original length. We utilize this mechanism to achieve remote and precise control of the filament locomotion via IR light. It is noted that an intensity of the broad-band IR light as low as 1 W cm^{-2} is sufficient to trigger the actuation due to the high loading of CNTs in the composite filaments, which is much smaller than most required light intensities reported in literature.^[17,27] Importantly, the actuation temperature does not change much after doping CNTs in LCEs.^[28]

Ideally, the actuators should achieve high work capacity while maintaining their adaptivity and compliance for soft robotics. As shown in Figure 4a,b, different weights are hanged under a single LCE/CNT composite filament and fixed by a clip. By turning the IR lamp on and off, the filament can reversibly lift up and drop off the weights, generating work during this process. The work capacity can be calculated as the work done (J) (force exerted times distance traveled) divided by the mass of the filament (kg). As shown in Figure 4b, a single 2 wt% CNT-doped

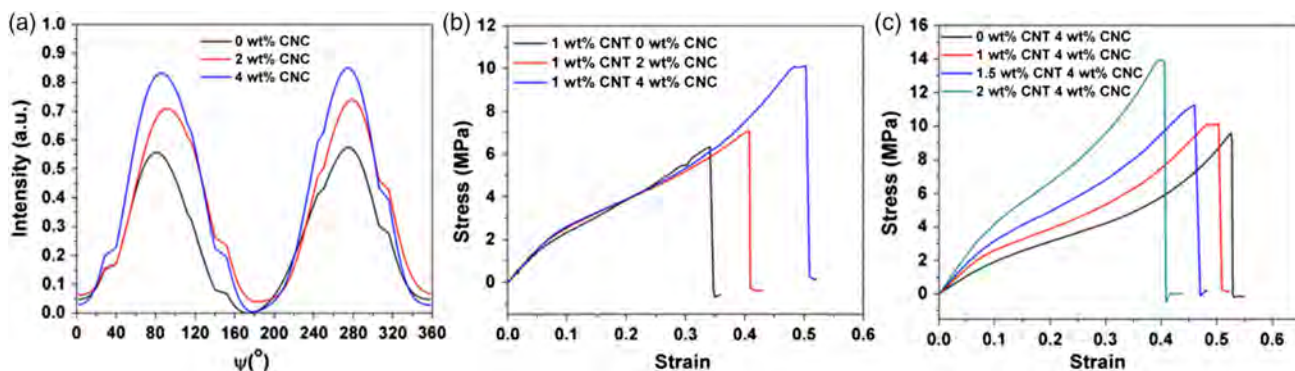


Figure 3. Effect of CNC and CNT concentrations in LCE/CNT composite filaments to LC alignment and mechanical properties, respectively. a) WAXRD azimuthal profiles of the composite filament with varying CNC concentration. b) Stress–strain curves of varying CNC concentration but fixed CNT concentration (1 wt%). c) Stress–strain curves of varying CNT concentration and fixed CNC concentration (4 wt%).

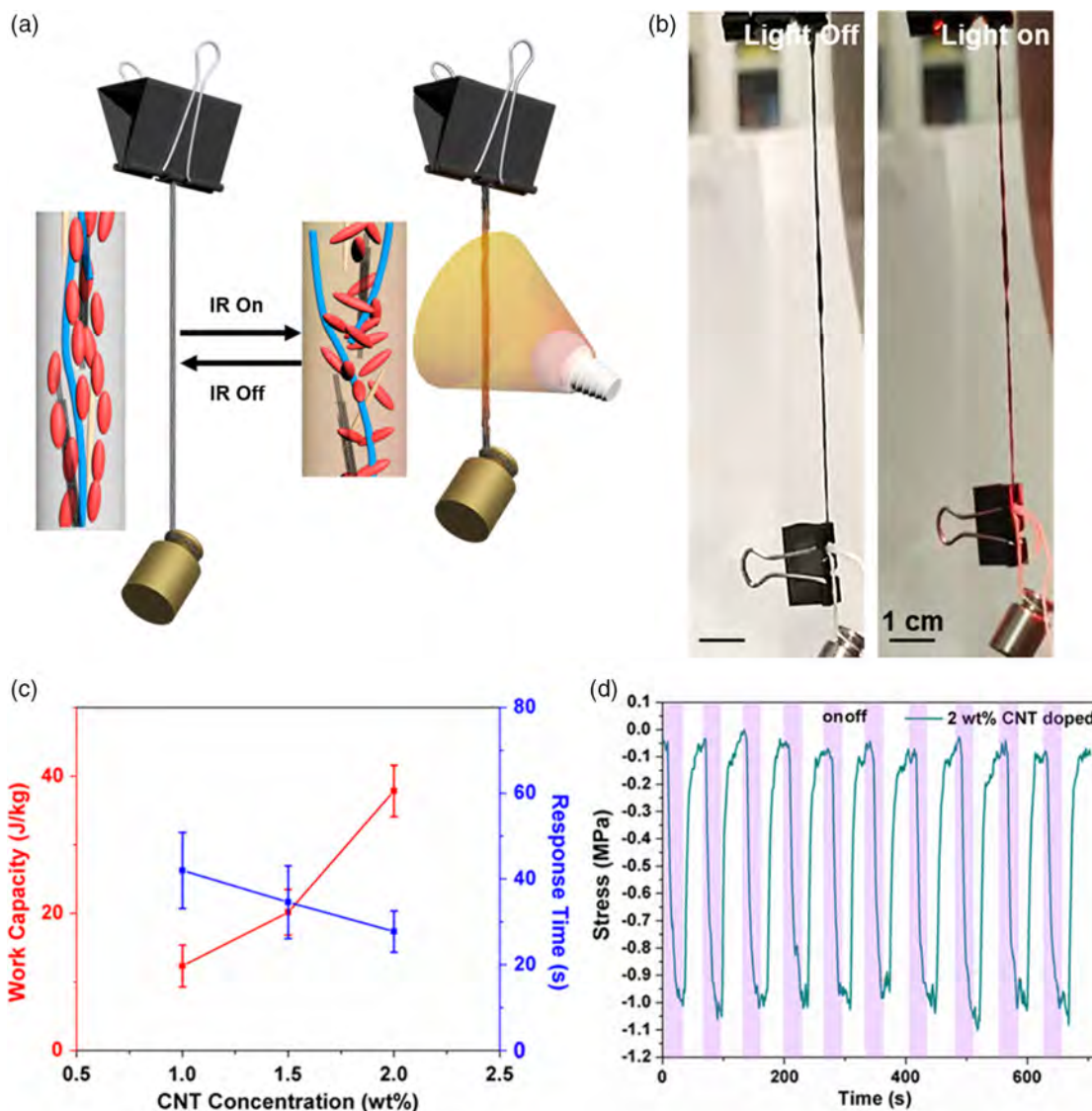


Figure 4. Photothermal effect and IR-responsive actuation of LCE/CNT composite filaments. a) Schematic illustration of photothermal effect and reversible actuation of filaments by IR light. b) Digital images of the reversible actuation of 2 wt% CNT-doped LCE filament lifting a 6.1 g object. Scale bars in both images are 1 cm. c) Work capacity (red) and response time (blue) of LCE/CNT composite filaments lifting objects of different weights as a function of doped CNT concentration. d) Actuation stress of 2 wt% CNT-doped LCE filament when IR light is periodically turned on and off over ten cycles.

LCE filament can lift a weight that is ≈ 560 times of its own weight. Attributed to the enhanced stiffness and modulus provided by CNTs with slight sacrifice of strain, the work capacity of LCE/CNT composite filaments increase from 12 J kg^{-1} with 1 wt% CNTs to 38 J kg^{-1} with 2 wt% CNTs (Figure 4c), which is comparable with that of the mammal skeletal muscle ($\approx 40 \text{ J kg}^{-1}$),^[18] and an order of magnitude larger than that of a pure LCE film.^[6] When four LCE/CNT filaments (2 wt% CNT) are physically bundled together, the work capacity increases to 55 J kg^{-1} (Figure S5, Supporting Information), possibly because the weight is more evenly distributed among filaments to avoid unnecessary breakage at the clip due to stress concentration. Moreover, we observe an increase in the actuation speed with higher CNT loadings: the response time of 2 wt%

CNT-doped LCE filament to IR lamp decreases to 28 s compared with 42 s from 1 wt% CNT-doped one (Figure 4c), whereas their recovery speeds remain similar (Figure S6, Supporting Information). The faster actuation speed could be explained by the increased thermal conductivity in LCE/CNT composites, as the increased CNT concentrations would lead to increased surface area of the CNTs, which effectively decreases the heat transfer distance among the CNTs.^[29] In the recovery process, however, the heat transfer is dominated by the filament surface, which remains similar for all CNT concentrations.

We then measure the actuation stress by dynamical mechanical analysis (DMA) (Figure 4d, Figure S7, Supporting Information). The filament is fixed at a small strain of 0.1% to ensure the slightly stretched state before measurement. The

IR light is turned on and off with approximately same time intervals and the stress is recorded in situ for ten cycles with little change, manifesting the reversible shape memory effect of LCEs as a result of their well-aligned mesogens in the polymer network. As shown in Figure 4d, the LCE/CNT composite filament with 2 wt% CNT loading could generate a maximum stress of 1.02 MPa reversibly, more than twice the amount of stress (0.48 MPa) from 1 wt% CNT-doped filament (Figure S7, Supporting Information).

2.4. Photothermal Responsive Soft Intelligent Systems

To demonstrate potential applications of LCE/CNT composite filaments as embedded intelligence in soft robotic systems, we choose the filament with the largest work capacity, i.e., 4 wt% CNCs and 2 wt% CNTs in LCE. Previously, it has been shown that when LC directors are aligned in a concentric ring geometry, a +1 topological defect is formed at the center. When heated

above T_{NI} , the azimuthal contraction along the LC director and the radial expansion around the defect center lead to the formation of a cone that has been shown for weight-lifting.^[6,9] To precisely control the LC molecular alignment in this pattern, great efforts have been made in the past including photoalignment,^[9] use of patterned microchannels,^[6] and 3D printing.^[15] However, the pattern resolution and sample dimension is highly dependent on the fabrication techniques.

Here, we can create an arbitrary 2D pattern by winding one single filament, e.g., into a spiral structure, which can be fixed by a small amount of uncured LCE ink (Figure 5a,b); the dimension of the pattern only depends on the length of the filament. As a result, the spiral pattern (1.4 cm in diameter) can buckle up into a cone with a stroke of 1 cm under IR light irradiation, which is approximately ten times of its original thickness (Figure 5c–d; Video S1, Supporting Information). We further utilize the meter-long length advantage of our composite filaments as well as the versatility to assemble them into any arbitrary structure, and demonstrate a manually woven pattern (Figure 5e–f). Under

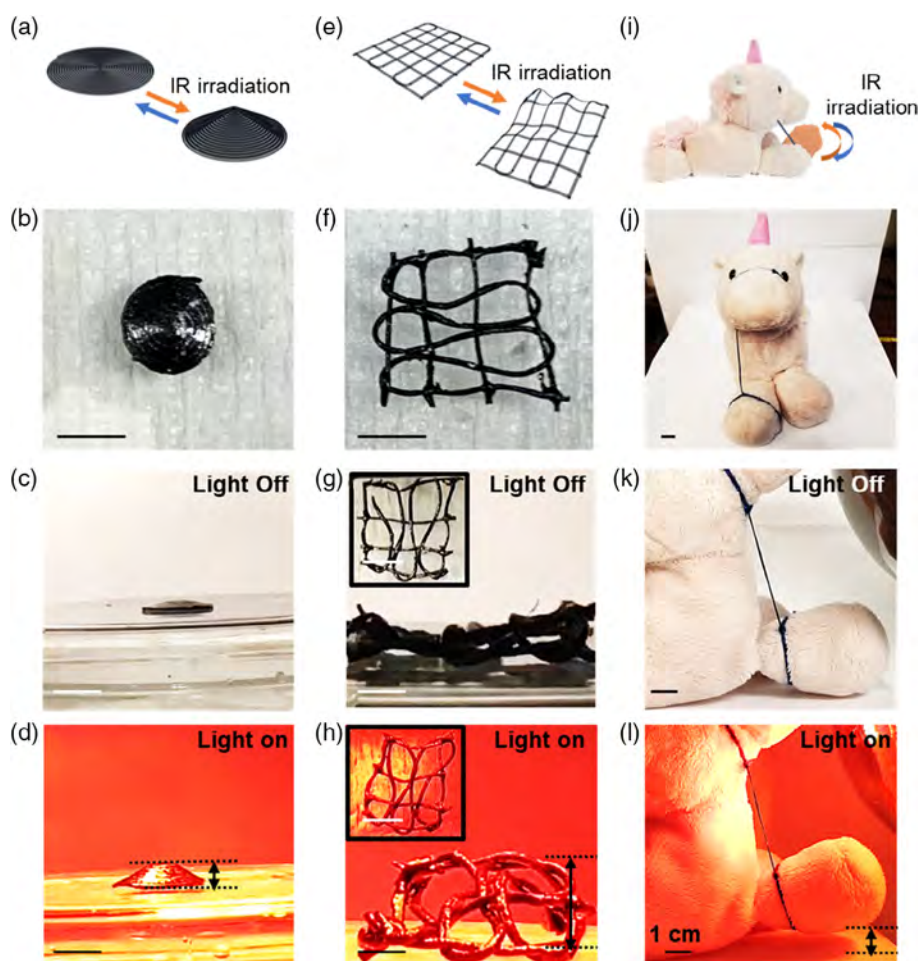


Figure 5. Photothermal responsiveness of LCE/CNT composite filaments (2 wt% CNT doped) in different geometries and patterns. a–d) a spiral pattern. e–h) a weaving pattern. i–l) a single filament connected to a plush unicorn. a,e,i) Schematic illustrations of photothermal responsiveness of the filament actuators. b,f,j) Digital images of LCE/CNT composite filaments function as different actuators. c,g,k) Side view digital images of LCE/CNT composite filament actuators when IR light is off. Inset in g) is top view. d,h,l) Side view digital images of LCE/CNT composite filament actuators when IR light is on. The actuation stroke indicated by the arrows in d,h,l) are 1, 1.97, and 1 cm, respectively. Inset in h) is the top view. Scale bar in (l) applies to all digital images.

IR irradiation, the contraction of filaments along the long axis results in the shrinkage in the overall size of the loosely woven pattern, decreasing in the sample dimension by $\approx 15\%$ (Figure 5g–h insets; Video S2, Supporting Information). We note that due to the imperfection of manual fabrication, residual stress in the pattern could cause the out-of-plane deformation as shown in Figure 5h and Video S3, Supporting Information.

Compared with 2D films, our 1D LCE/CNT composite filaments exhibit one more degree of freedom, thus are ideal for tasks that require system-level integration of actuators. The composite filaments, either single strand or bundled, can be connected to any arbitrary parts of the robotic systems, much like the muscle fibers in the animal musculoskeletal system, which can deform individually or collaboratively to achieve programmable and well-controlled complex locomotion.

For proof-of-concept, we integrate one single filament with a plush unicorn (Figure 5i,j). The two ends of the filament are tied on the head and one foot of the unicorn, respectively. In this way, the unicorn foot can be repeatedly lifted up by 1 cm when IR light is on and be dropped back when light is off, mimicking the hopping motion (Figure 5k,l; Video S4, Supporting Information). Following this simple design, we expect that this plush unicorn can be turned into a remotely controlled soft robot, where filaments can be integrated at arbitrary positions of the unicorn body to create in-phase or out-of-phase locomotion. To better control

the dynamic behaviors of the robotic systems, we resort to the electrothermal effect such that we can potentially use the electrical circuitry and motors to control the locomotion.

2.5. Electrothermal Responsive Soft Intelligent Systems

Electrically powered actuators are desirable for many practical applications due to their obvious advantages, including system-level integration and controllability, and energy efficiency.^[30] One approach to realize electrical responsiveness is based on Joule heating, where the passage of an electric current through a conductor releases heat.^[31] Joule heating has been widely incorporated into responsive soft materials to provide electrothermal responsiveness,^[32] because it requires much lower voltage compared with other electroactive materials such as dielectric elastomers.^[18] Here, we choose thin copper wires (diameter = $20\ \mu\text{m}$) as the Joule heater, as they are highly conductive, easy to handle, whereas soft enough not to influence the deformation of the LCE/CNT composite filaments. To test the feasibility of this approach, a copper wire is curved into a “S” shape and attached to the back of the spiral pattern assembled from an LCE/CNT composite filament (Figure 6a, Figure S8a, Supporting Information). When the voltage is on, the Joule heat generated raises the temperature above the phase transition of the LCE network, buckling the spiral pattern into a cone (Figure 6c, Video S5,

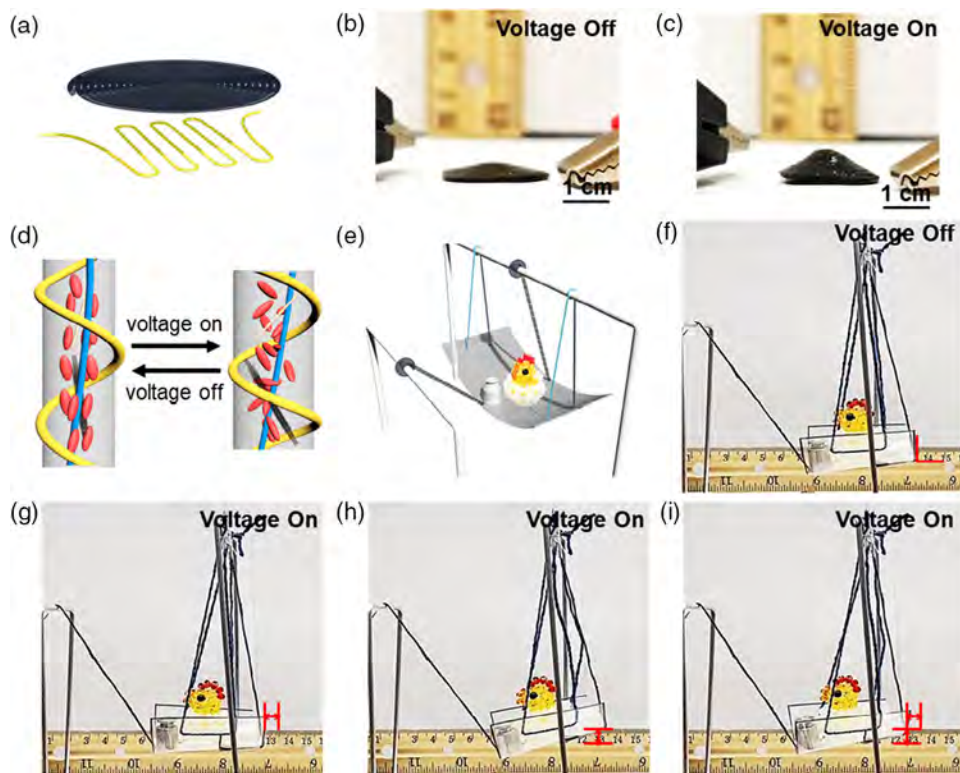


Figure 6. Electrothermal responsiveness of LCE/CNT composite filaments (2 wt% CNT doped) function as different soft intelligent systems. a) Schematic illustration of a spiral pattern with attached copper wires. b) Side view digital image of LCE/CNT composite filament actuator when voltage is off. c) Side view digital image of LCE/CNT composite filament actuator when voltage is on. d) Schematic illustration of the electrothermal actuation of a filament with copper wires based on joule heating effect. e) Schematic illustration of a swing with two individually controllable swinging directions. The weight and the chicken are both 10 g. f) Side view digital image of the swing when voltage is off. g–i) Side view digital image of the swing when voltage is on. Red bars indicate swinging distances. g) swing to the front; h) swing to the top; i) swing to both the front and the top.

Supporting Information). The spiral pattern could recover to the flat state when the voltage is switched off and heat dissipates (Figure 6b). The maximum buckling height of the cone is 1 cm, which is the same as the height under IR irradiation, indicating that copper wires do not interfere with the actuation performance of the composite filaments.

Next, we build up an intelligent swing set that can perform three controllable swing motions using two LCE/CNT composite filaments. The copper wires are periodically wound onto the filaments, so that the filaments undergo reversible deformation along the long axis via voltage control (Figure 6d). Two filaments are attached to the front and top stands, respectively, and a 10 g plastic chicken together with an additional 10 g weight (total weight of 20 g) serve as the passenger on the swing (Figure 6e, Figure S8b, Supporting Information). The filaments are controlled by two separate power sources, so they can be actuated individually to pull the swing to the front or to the top. As shown in Figure 6g,h, the displacement is 6 mm to the front and 8.5 mm to the top. When both filaments are actuated by power supplies, the chicken and weight experience synchronized motions—swinging to the front and to the top with the same amount of displacement (Figure 6i). The entire procedure is shown in Video S6, Supporting Information, with each motion repeated five times.

Although electrothermal actuation of LCE/CNT composite filaments is ultimately triggered by heat, it is much faster than photothermal actuation due to the more concentrated heating and energy input. We adopt the same method to wind a copper wire around a composite filament and attach the filament to a self-balanced eagle (Figure S8c, Video S7, Supporting Information). The contraction of the filament allows the eagle to fly downward with an average speed of 10 s, which is almost three times faster than that of the photothermal actuation (28 s), presumably because copper wires have higher heat transfer efficiency than the photothermal effect provided by IR light. The recovery process is also faster, as electrothermal heating is local and the heat dissipation is more efficient, whereas the surrounding environment is also heated during the IR light actuation. In the case of the electrothermally actuated flying eagle, the average recovery speed is 20 s, half of the time by IR light actuation, 43 s.

3. Conclusion

In conclusion, we have fabricated extrusion-based LCE/CNT composite filaments in a scalable manner. The nanofiller CNCs facilitate the alignment of LC molecules along the filament long axis, whereas the extrusion process enables high loading of CNTs in LCE matrix without aggregation, resulting in enhanced mechanical robustness and faster actuation speed. The LCE/CNT composite filaments exhibit both photothermal and electrothermal responsiveness with a maximum work capacity of 38 J kg^{-1} , comparable to the value of mammal skeletal muscles. The actuations are reversible, fast, and can be integrated into different systems to induce shape transformation and locomotion. This work demonstrates the versatility of filament-based actuators, whereas the LCE composites can generate both agile and forceful actuation, which opens the door to create multifunctional soft intelligent systems.

4. Experimental Section

Materials: LC monomer RM82 was purchased from Wilshire Technologies. 1,3-PDT was purchased from Sigma-Aldrich, and RM82–1,3 PDT was synthesized following the literature.^[7] Photoinitiator, 2,2-dimethoxy-2-phenylacetophenone (DMPA) was purchased from Ark Pharm. CNCs (5–20 nm wide, 150–200 nm long) was purchased from The University of Maine Process Development Center. Multiwall carbon nanotubes (MWCNTs, inner diameter 3–5 nm; outer diameter 8–15 nm; length 10–50 μm) was purchased from Cheaptubes. All chemicals were used as received without further purification.

Fabrication of LCE/CNT Composite Filaments: RM82 and RM82–1,3 PDT were mixed at 1:1 molar ratio in a glass vial, together with 2 wt% DMPA as photoinitiator, and the two nanofillers, MWCNTs (from 0 to 2 wt%), and CNCs (from 0 to 4 wt%) at room temperature. The mixture was then heated to 120 °C and stirred for 5 min before it was loaded into a plastic syringe. The syringe was heated at 80 °C in the oven for 30 min to enable the oligomerization of the reactants. Oligomerized LCE ink was extruded by a Harvard Apparatus Pump 11 Elite syringe pump at a constant speed of $50 \mu\text{L min}^{-1}$. The syringe pump was fixed in an upright position so that the nozzle can face the ground. The 365 nm UV light was provided by LED4D067 4-wavelength high-power LED source operated by a DC4104 driver from Thorlabs. The UV light at an output power of 85 mW cm^{-2} was irradiated at the nozzle tip to cure the extruded mixture into the filament shape before it was collected by a rotating mandrel (Tong Li Tech) located below the nozzle. The mandrel rotated at a constant speed of 2 rad min^{-1} . After extrusion, the fabricated filaments were removed carefully from the mandrel using tweezers and underwent flood UV exposure at a total dosage of 100 J cm^{-2} to completely cure the LCE filaments.

Tensile Testing: The tensile tests were performed on an Instron 5564 model, and a tensile load cell with capability of 10 N was used. All the samples had the same initial length before testing (10 cm) and pulled till breakage. The speed of the moving load cell was fixed at 5 mm min^{-1} . The stress–strain curve was calculated from the force–displacement curve obtained, the diameter, and the initial length of the filaments.

Dynamic Mechanical Analysis: DMA test was performed on an ARES-G2 rheometer. The filament was manually mounted on the linear fiber tension holder. The holders were moved apart slowly until a negative axial force observed to ensure the filament was straight and slightly in tension. The strain was then fixed while the axial force was recorded over time and the IR light was turned on and off periodically to activate the reversible contraction of the LCE/CNT composite filament.

Wide-Angle X-Ray Diffraction: The X-ray diffraction pattern was collected by the Xeuss 2.0 Dual Source and Environmental X-ray Scattering system with copper source using an X-ray beam of 1.54 Å wavelength, 50.0 kV, 0.60 mA. The sample chamber was under the vacuum environment at 20 °C. All data were collected at a sample-to-detector distance of 322 mm, and calibrated by silver behenate standard. Each sample was conducted under the 600 s exposure. The data analysis and transformation were done in the Foxtrot analysis software.

Optical and Electron Microscope Images: The cross-sectional SEM images were obtained from FEI Quanta 600 environmental scanning electron microscopy (ESEM) at 15 kV electron beam. The reflection mode optical images were taken by an Olympus BX61 Motorized Microscope. All digital images were taken by iPhone 11 Pro Max.

Work Capacity and Response Time: Work capacity (J kg^{-1}) can be calculated as the work done (J) (force exerted times distance travelled) divided by the mass of the filament (kg). The distance traveled was obtained from the actuation videos. The response time of IR actuation was averaged from DMA data, and the response time of electrothermal actuation was averaged from Video S7, Supporting Information.

Photothermal and Electrothermal Actuations: The IR lamp was purchased from SATCO with an Impact Is-6b light stand. The intensity of the IR lamp was approximately 1 W cm^{-2} . For the IR light-actuated spiral pattern and weaving pattern, a petri dish containing deionized (DI) water was put underneath the composite filament pattern for more efficient heat dissipation during the recovery process. The power supply for electrothermal actuation was model QRD 20-4 from Sorensen. The voltage

was 8 V and the current was 1.6 A. All the actuation performance videos were taken by iPhone 11 Pro Max.

Supporting Information

Supporting Information is available from the Wiley Online Library or from the author.

Acknowledgements

J.L. and Y.G. contributed equally to this work. The research is supported by Army Research Offices (ARO) through the MURI program, ARO #W911-NF-1810327 (Topic Chief, Samuel Stanton), National Science Foundation (NSF) through the University of Pennsylvania Materials Research Science and Engineering Center (MRSEC) (DMR-1720530), and Center for Engineering MechanoBiology (CEMB) (CMMI-1548571). The authors gratefully acknowledge the use of SEM supported by NSF MRSEC.

Conflict of Interest

The authors declare no conflict of interest.

Keywords

carbon nanotube composite filaments, electroresponsive, liquid crystal elastomers, photoresponsive, soft robots

Received: December 3, 2019

Revised: December 17, 2019

Published online: February 18, 2020

- [1] D. Rus, M. T. Tolley, *Nature* **2015**, 521, 467.
 [2] Y. S. Zhang, A. Khademhosseini, *Science* **2017**, 356, eaaf3627.
 [3] A. Lendlein, O. E. C. Gould, *Nat. Rev. Mater.* **2019**, 4, 116.
 [4] T. J. White, D. J. Broer, *Nat. Mater.* **2015**, 14, 1087.
 [5] S. V. Ahir, A. R. Tajbakhsh, E. M. Terentjev, *Adv. Funct. Mater.* **2006**, 16, 556.
 [6] Y. Xia, G. Cedillo-Servin, R. D. Kamien, S. Yang, *Adv. Mater.* **2016**, 28, 9637.
 [7] Y. Xia, X. Zhang, S. Yang, *Angew. Chem. Int. Ed.* **2018**, 57, 5665.
 [8] H. Aharoni, Y. Xia, X. Zhang, R. D. Kamien, S. Yang, *Proc. Natl. Acad. Sci.* **2018**, 115, 7206.
 [9] T. H. Ware, M. E. McConney, J. J. Wie, V. P. Tondiglia, T. J. White, *Science* **2015**, 347, 982.
 [10] S. Ahn, T. H. Ware, K. M. Lee, V. P. Tondiglia, T. J. White, *Adv. Funct. Mater.* **2016**, 26, 5819.
 [11] T. Guin, M. J. Settle, B. A. Kowalski, A. D. Auguste, R. V. Beblo, G. W. Reich, T. J. White, *Nat. Commun.* **2018**, 9, 2531.
 [12] M. O. Saed, C. P. Ambulo, H. Kim, R. De, V. Raval, K. Searles, D. A. Siddiqui, J. M. O. Cue, M. C. Stefan, M. R. Shankar, T. H. Ware, *Adv. Funct. Mater.* **2019**, 29, 1806412.
 [13] A. Kotikian, R. L. Truby, J. W. Boley, T. J. White, J. A. Lewis, *Adv. Mater.* **2018**, 30, 1706164.
 [14] M. López-Valdeolivas, D. Liu, D. J. Broer, C. Sánchez-Somolinos, *Macromol. Rapid Commun.* **2018**, 39, 1700710.
 [15] C. P. Ambulo, J. J. Burroughs, J. M. Boothby, H. Kim, M. R. Shankar, T. H. Ware, *ACS Appl. Mater. Interfaces* **2017**, 9, 37332.
 [16] H.-F. Lu, M. Wang, X.-M. Chen, B.-P. Lin, H. Yang, *J. Am. Chem. Soc.* **2019**, 141, 14364.
 [17] H. Kim, J. A. Lee, C. P. Ambulo, H. B. Lee, S. H. Kim, V. V. Naik, C. S. Haines, A. E. Aliev, R. Ovalle-Robles, R. H. Baughman, T. H. Ware, *Adv. Funct. Mater.* **2019**, 29, 1905063.
 [18] P. Brochu, Q. Pei, *Macromol. Rapid Commun.* **2010**, 31, 10.
 [19] D. J. Roach, X. Kuang, C. Yuan, K. Chen, H. J. Qi, *Smart Mater. Struct.* **2018**, 27, 125011.
 [20] R. Hagenmueller, H. H. Gommans, A. G. Rinzler, J. E. Fischer, K. I. Winey, *Chem. Phys. Lett.* **2000**, 330, 219.
 [21] J. E. Marshall, Y. Ji, N. Torras, K. Zinoviev, E. M. Terentjev, *Soft Matter* **2012**, 8, 1570.
 [22] T. Guin, B. A. Kowalski, R. Rao, A. D. Auguste, C. A. Grabowski, P. F. Lloyd, V. P. Tondiglia, B. Maruyama, R. A. Vaia, T. J. White, *ACS Appl. Mater. Interfaces* **2018**, 10, 1187.
 [23] J. P. F. Lagerwall, C. Schütz, M. Salajkova, J. Noh, J. Hyun Park, G. Scalia, L. Bergström, *NPG Asia Mater.* **2014**, 6, e80.
 [24] P.-X. Wang, W. Y. Hamad, M. J. MacLachlan, *Nat. Commun.* **2016**, 7, 1.
 [25] R. R. Kohlmeier, J. Chen, *Angew. Chem. Int. Ed.* **2013**, 52, 9234.
 [26] K. Mizuno, J. Ishii, H. Kishida, Y. Hayamizu, S. Yasuda, D. N. Futaba, M. Yumura, K. Hata, *Proc. Natl. Acad. Sci.* **2009**, 106, 6044.
 [27] X. Lu, H. Zhang, G. Fei, B. Yu, X. Tong, H. Xia, Y. Zhao, *Adv. Mater.* **2018**, 30, 1706597.
 [28] Y. Ji, Y. Y. Huang, R. Rungsawang, E. M. Terentjev, *Adv. Mater.* **2010**, 22, 3436.
 [29] M. Moniruzzaman, K. I. Winey, *Macromolecules* **2006**, 39, 5194.
 [30] Q. He, Z. Wang, Y. Wang, A. Minori, M. T. Tolley, S. Cai, *Sci. Adv.* **2019**, 5, eaax5746.
 [31] J.-H. Jeong, T. Jin Mun, H. Kim, J. Hwan Moon, D. Weon Lee, R. H. Baughman, S. Jeong Kim, *Nanoscale Adv.* **2019**, 1, 965.
 [32] Y.-Y. Xiao, Z.-C. Jiang, X. Tong, Y. Zhao, *Adv. Mater.* **2019**, 31, 1903452.